ELSEVIER

Journal of Nuclear Materials 313–316 (2003) 947–951

journal of nuclear materials

www.elsevier.com/locate/jnucmat

Asymmetric divertor plasma distribution observed in Heliotron J ECH discharges

T. Mizuuchi [a,*], W.L. Ang [b], Y. Nishioka [b], T. Kobayashi [b], K. Nagasaki [a], H. Okada [a], K. Kondo [b], F. Sano [a], S. Besshou [b], Y. Nakamura [b], M. Nakasuga [b], Y. Manabe [b], H. Shidara [b], H. Kawazome [b], S. Maeno [b], T. Takamiya [b], M. Takeda [b], K. Tomiyama [b], H. Tsuru [b], Y. Ohno [b], H. Kubo [b], H. Yukimoto [b], M. Iriguchi [b], T. Obiki [a]

[a] *Institute of Advanced Energy, Kyoto University, Gokasho 611-0011, Uji, Japan*
[b] *Graduate School of Energy Science, Kyoto University, Gokasho, Japan*

Abstract

An asymmetric divertor plasma distribution observed in the standard configuration of Heliotron J is reported. The divertor plasma profiles were investigated with two Langmuir probe arrays, which were installed at the geometrically up–down symmetric positions, for three different heating schemes of ECH with 53.2 or 70 GHz microwaves. Although the position of the divertor plasma flux was almost consistent with the footprint position of the divertor field lines, the existence of two types of up–down asymmetry was revealed in the divertor plasma density and floating potential profiles. The first type of asymmetry was mainly observed near the boundary to the 'private region'. This asymmetry seems to be independent of the heating schemes of the toroidal position of the heating source. As the direction of the confinement field was reversed, the feature of the plasma profile on the top array came to appear on the bottom array, and vice versa. This field-direction dependence indicates that the asymmetric $\boldsymbol{B} \times \nabla B$ drift motion of charged particles might cause this type of asymmetry. The second type of asymmetry was observed in the region away from the boundary and seemed to depend on the heating schemes.

PACS: 52.55.Hc
Keywords: Divertor asymmetry; Helical-axis heliotron; Heliotron J; Current-less plasma; ECH; $\boldsymbol{B} \times \nabla B$ drift

1. Introduction

A divertor is one of the essential components for a fusion reactor. From a viewpoint of the divertor heat load and particle flux handling, it is important to understand and control the divertor flux distribution. Especially, the existence of the divertor flux asymmetry in its amount or the distribution profile is a crucial issue for the divertor design. In tokamak divertors, the existence of 'in–out' asymmetry of the divertor flux is usually observed. In TEXT-Upgrade, 'up–down (or vertical)' asymmetry is also observed in the legs, which are located geometrically symmetric positions about the midplane [1]. In helical devices, where the divertor is designed based on its topological feature of the edge field lines, asymmetric distributions of the diverted plasma were also reported [2–4]. The geometrical or topological asymmetries of the divertor field structure itself can explain some of the observed asymmetric distributions in the helical devices. However, there still remains 'unexpected' asymmetry like the up–down asymmetry in geometrically

* Corresponding author. Tel.: +81-774 38 3451; fax: +81-774 38 3535.
E-mail address: mizuuchi@iae.kyoto-u.ac.jp (T. Mizuuchi).

0022-3115/03/$ - see front matter
PII: S0022-3115(02)01392-2

symmetric legs. In Heliotron E (an $\ell = 2$ heliotron device), a strong up–down asymmetry in the divertor plasma flux was observed for NBI, ECH and NBI + ECH plasmas. The dependence of the divertor asymmetry on several external conditions such as the direction of the confinement field, the heating method, heating power and toroidal position of the heating source was investigated [3]. Theoretical works on direct losses of energetic trapped particles from the confinement region were also performed [5] and inferred that the divertor flow asymmetry observed in Heliotron E was related to convection-like losses of fast ions or electrons enhanced by the vertically asymmetric field ripples [6]. It is also predicted that the effect of the radial electric field and its shear on escaped particle orbits can change the asymmetry [6]. In the Uragan-3M torsatron, a strong up–down asymmetry of the divertor plasma flux was also investigated for ICRF plasmas and it is concluded that the asymmetry is simply related to direct (non-diffusive) losses of charged particles from the core region affected by the ion toroidal $\boldsymbol{B} \times \nabla B$ drift [4].

This paper reports the divertor plasma distribution and its up–down asymmetric profile observed in ECH plasmas under the standard configuration of Heliotron J. This device can flexibly control the edge field topology and the standard configuration provides a helical divertor type configuration [7]. The footprints of 'divertor' field lines on the wall surface are localized not only in the poloidal direction but also in the toroidal direction. This exhibits a striking contrast to that of the conventional helical divertor field in a planer-axis heliotron device such as Heliotron E [8] and LHD [9]. The positions where the field lines starting near the last closed flux surface cross the wall surface depend on the direction of field-line tracing (clockwise or counter-clockwise direction), suggesting that the parallel and anti-parallel flows of the SOL plasma reach to the different locations.

2. Experimental setup

Heliotron J is a flexible $\ell = 1/m = 4$ helical-axis heliotron device. The main characteristics [10] are the reduction of the neoclassical diffusion coefficient in $1/\nu$ regime and the favorable MHD characteristics with the magnetic well, which are coming from the strongly modulated helical magnetic axis [11]. The averaged major and minor radii of the plasma are $\langle R \rangle = 1.2$ m and $\langle a \rangle = 0.17$–0.18 m, respectively. In this study, current-free hydrogen plasmas were produced by the second harmonic ECH with a 53.2 GHz system at $\langle B \rangle \approx 0.95$ T or a 70 GHz system at $\langle B \rangle \approx 1.25$ T in the standard configuration. In addition, the ECH plasma was successfully produced using the 53.2 GHz system also for the higher magnetic field ($\langle B \rangle \approx 1.4$–$1.5$ T). In this high field operation, there is no resonance layer for the ECH waves in the core region. The electron Bernstein wave heating is supposed as a plausible heating mechanism [7,12]. In the 53.2 GHz system, the microwaves of the axisymmetric TE_{02} mode from three gyrotrons were injected with oversized waveguide launchers. Two oblique injection launchers are located at $\phi \approx 129°$ and a single launcher for almost perpendicular injection is located at $\phi \approx 223°$ as shown in Fig. 1. The pulse width and the maximum power were 40–50 ms and $P_{\mathrm{ECH}} \leqslant 0.4$ MW, respectively. The 70 GHz ECH system injected a single beam (TEM_{00} mode, $P_{\mathrm{ECH}} \leqslant 0.4$ MW, ≈200 ms) with a diameter of about 40 mm in the e^2-folding power at the plasma center in the perpendicular injection scheme. The launcher of this 70 GHz system ($\phi \approx 315°$) has a steering mirror to change the injection angle in the toroidal and poloidal directions. A condition for almost perpendicular on-axis heating was selected in this experiment. Typical ranges of the core electron density and temperature of the ECH plasmas were $\bar{n}_{\mathrm{e}} \sim 0.2$–$3 \times 10^{19}$ m^{-3}, $T_{\mathrm{e}} \sim 0.2$–1.0 keV, respectively.

The edge plasma was monitored with three Langmuir probe systems [13]. One is a movable array at $\phi = 247.5°$ for the SOL plasma and the other two are fixed probe arrays near the wall for the divertor plasma. In the standard configuration, the footprints of the divertor flux bundles on the vacuum chamber wall are concentrated in four regions par a pitch of the confinement field (two on the high field side and the other two on the low field side) [7]. The fixed probe arrays are installed at the geometrically up–down symmetrical positions in a part of the low field side footprint areas, $\phi = 67.5°$ (top, #3.5 array) and 112.5° (bottom, #5.5 array). First, we used two-dimensional array sets with 28 pins (7 the poloidal direction × 4 the toroidal direction) as

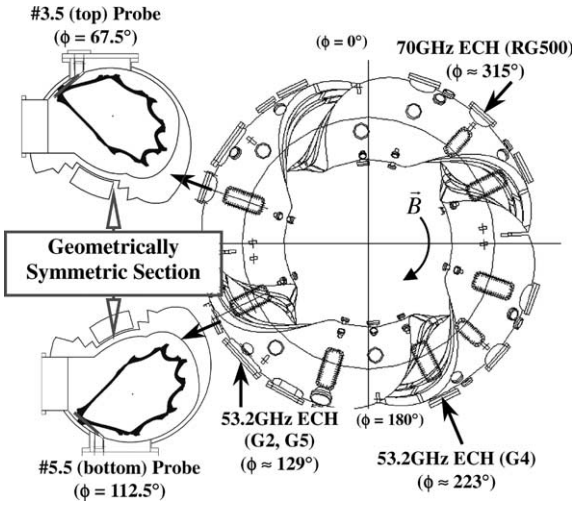

Fig. 1. Top view of Heliotron J showing the ECH launchers and probe positions. The inserts are the poloidal cross-sections at the probe positions and Poincaré-plots of the edge field lines.

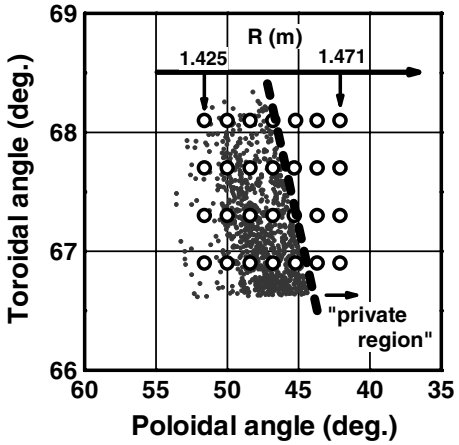

Fig. 2. Footprints of the divertor field lines on the #3.5 (7 × 4)-array (●). The positions of the electrode are indicated by (○).

the fixed probe array to check the consistency of the divertor plasma distribution and the calculated footprint position of the divertor field lines. Then, we changed to new arrays with 21 electrodes along the poloidal direction to measure wider range in this direction. The bias voltage for the electrodes was swept with a frequency of 200 Hz and I_s, T_e and V_f were evaluated from the V–I characteristic curve based on the usual single probe model.

The calculated footprints of the divertor field lines on the #3.5 (7 × 4) array are shown in Fig. 2. In the 'private region' (the no-dots region on the right side area in Fig. 2), the connection length of the field line, L_w, rapidly decreases. On the left side, however, L_w is kept long (~40–100 m) up to the end of this probe set.

3. Profile of divertor plasmas

3.1. 53.2 GHz second harmonic ECH plasmas

For 53.2 GHz second harmonic ECH, the divertor plasma position was consistent with that expected from the connection length profile (see Fig. 14 in Ref. [14]). Relatively higher values of T_e and the density were obtained in the longer L_w region and measured poloidal shift of such plasma region along the toroidal direction was consistent with the expected shift of the footprint position from the field calculation. This L_w dependence of the divertor plasma distribution was much clearly observed on #5.5 (bottom) probe array. On #3.5 (top) array, the density did not decrease so much in the 'private region ($R > 1.46$ m)' compared to that on #5.5 array as shown in Fig. 3.

The up–down asymmetry of the divertor plasma was observed clearly in the floating potential profiles (the bottom figure in Fig. 3). On #5.5 (bottom) array, the

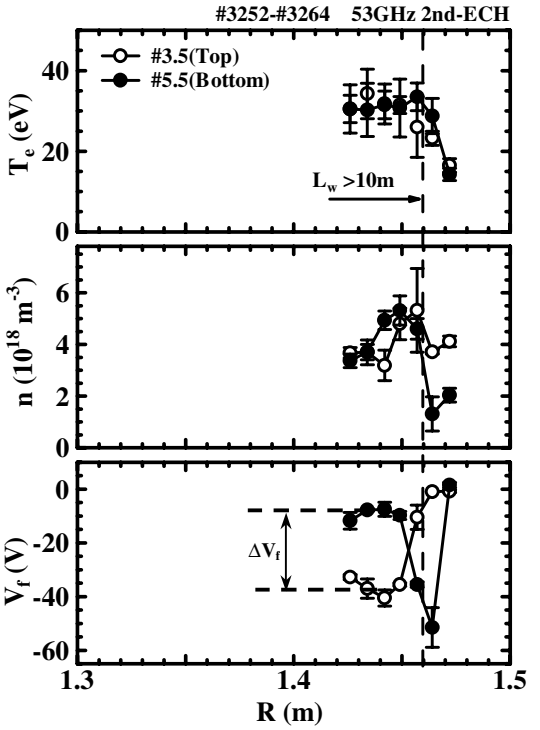

Fig. 3. Typical poloidal distribution of electron temperature (T_e), density (n) and floating potential (V_f) at the top and bottom probe arrays for 53.2 GHz second harmonic ECH plasma ($\langle B \rangle \approx 0.95$ T). The horizontal axis is scaled by the distance from the torus center instead of the poloidal angle.

floating potential, which was $V_f \approx 0$ V for $R > 1.46$ m, rapidly dropped to a large negative value near the boundary to the private region ($R \sim 1.46$ m) and then V_f came back to a relatively small negative value in the divertor footprint region ($R < 1.45$ m). On #3.5 (top) array, V_f smoothly decreased from the private region to a large negative value in the divertor footprint region.

These peculiarities of the density and V_f profiles observed on the top (bottom) array came to appear on the bottom (top) array as the direction of the confinement field was reversed [13].

3.2. 53.2 GHz high field ECH plasmas

An example of the divertor plasma profile for the 53.2 GHz high field ECH is shown in Fig. 4, where the plasma parameters were measured with the 21-pin arrays. The calculated divertor field bundle (e.g. the field lines with $L_w > 10$ m) crosses the probe array in the zone of 1.37 m < R < 1.46 m. As shown in the figure, relatively higher density and temperature and negative floating potential were observed in this zone for both probe arrays, indicating the main divertor plasma flux comes to the positions of the divertor field lines.

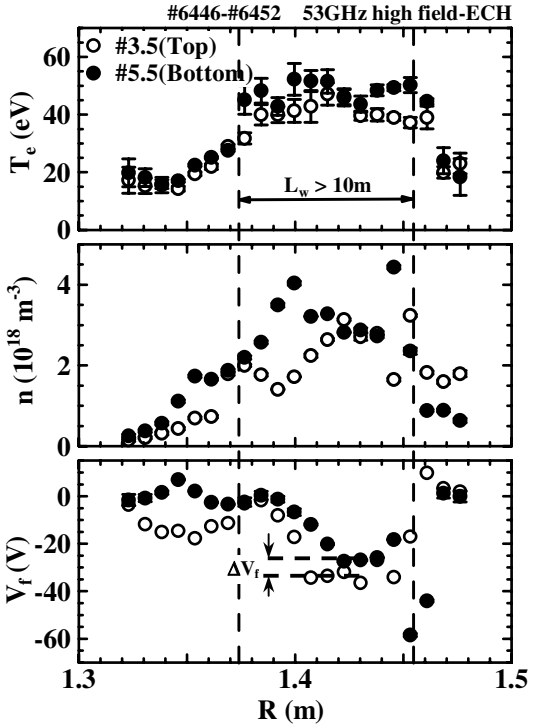

Fig. 4. Typical poloidal distribution of electron temperature (T_e), density (n) and floating potential (V_f) at the top and bottom probe arrays for 53.2 GHz high field ECH plasma ($\langle B \rangle \approx 1.42$ T).

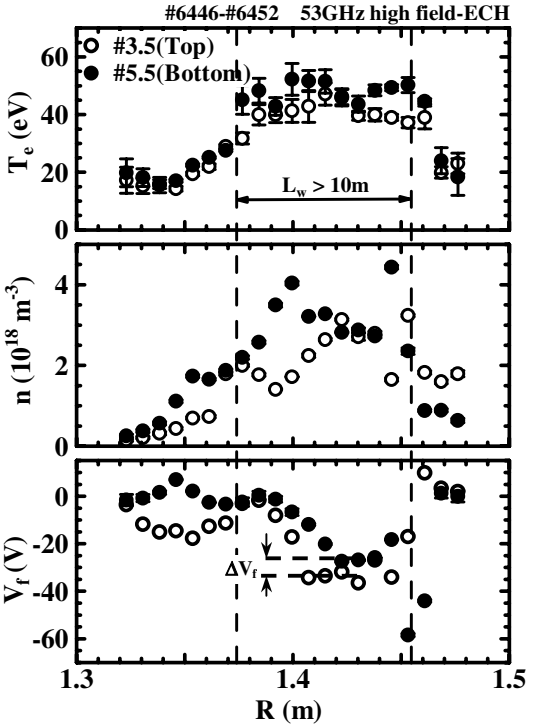

Fig. 5. Typical poloidal distribution of electron temperature (T_e), density (n) and floating potential (V_f) at the top and bottom probe arrays for 70 GHz second harmonic ECH plasma ($\langle B \rangle \approx 1.25$ T).

As for the up–down asymmetry in the region of 1.42 m < R < 1.48 m (corresponding the region measured with the 7×4 probe), almost the same characteristics of the density and floating potential profiles as those observed for the 53.2 GHz second harmonic ECH (Fig. 3) were also observed in this heating scheme. On #5.5 (bottom) array, V_f rapidly dropped near the private region boundary ($R \sim 1.45$ m) and recovered to a relatively small negative value, while V_f on #3.5 (top) array smoothly decreased to a large negative value. It is interesting to note that the difference in V_f between #3.5 (top) and #5.5 (bottom) arrays in the region of 1.42 m < R < 1.44 m seems to be small ($\Delta V_f \sim 10$ V) compared to that in the 53.2 GHz second harmonic ECH case ($\Delta V_f \sim 30$V).

In the region of $R < 1.42$ m, V_f on #5.5 (bottom) probe array gradually increases to ~0 V, while that on #3.5 array keeps a large negative value and rapidly increases to ~ 0 V from $R \approx 1.41$ m. It was also revealed that the radial dependence and the amount of the density on the top and bottom arrays were clearly different in the region of 1.38 m < R < 1.41 m. The density on #5.5 array is larger than that on #3.5 array. In this region, the R-profile of the density had the local maximum at $R \sim 1.4$ m on #5.5 (bottom) array, while it had the local minimum at $R \sim 1.39$ m on #3.5 (top) array.

3.3. 70 GHz second harmonic ECH plasmas

An example of the divertor plasma profile for the 70 GHz second harmonic ECH case is shown in Fig. 5. Almost the same asymmetric characteristics as those for the previous case were also observed. The difference in V_f between the two arrays was larger ($\Delta V_f \sim 20$V) than that for the previous case (Fig. 4) but smaller than that for the 53.2 GHz second harmonic ECH case (Fig. 3). The asymmetry in the density profile in the region of 1.38 m < R < 1.41 m was also observed but it seems rather mild.

4. Discussions and summary

The divertor plasmas for 53.2 GHz or 70 GHz ECH discharges in the Heliotron J standard configuration were investigated with two Langmuir probe arrays installed at the geometrically up–down symmetric positions. The main divertor plasma flux was observed in the

divertor filed footprint position. The existence of the up–down asymmetry in the divertor plasma distribution was revealed. The characteristics of the asymmetric profiles near the boundary to the private region were almost the same for 53.2 GHz second harmonic ECH, 53.2 GHz high field ECH and 70 GHz second harmonic ECH discharges. In the two 53 GHz ECH cases, the same launching system was used, but in the 70 GHz ECH case, the launching position and the injection mode of the microwave were different from those in the 53.2 GHz ECH cases. These facts indicate that the main characteristics of the asymmetry described in the Section 3 are insensitive to the heating schemes or the toroidal position of the heating source.

The characteristics of the asymmetries on the arrays were replaced each other when the direction of the confinement field was reversed. Such field-direction dependence was observed in other devices and indicating drift effects on the asymmetry. The asymmetric $\boldsymbol{B} \times \nabla B$ drift motion of charged particles is discussed in helical devices [4,6]. The qualitative discussions based on this drift effect on the divertor plasma flow were done to explain the asymmetric divertor plasma distribution on the 7×4 probe arrays [13]. A numerical examination of the $\boldsymbol{B} \times \nabla B$ drift effects on the divertor plasma profile for the Heliotron J configuration was also performed based on a non-collisional guiding center tracing. The asymmetric density distribution and its reversal with the magnetic field were reproduced in the calculation model [13].

Direct losses of energetic trapped particles have a vertical asymmetry and they can affect the divertor plasma asymmetry. Since the production rate and birth position of trapped electrons would be not the same for the three different heating schemes, the differences of ΔV_f for the three heating schemes might be related to such direct losses of the electrons. On the other hand, collision-less 'loss particle analysis' in the Heliotron J [15] shows that the footprints of the loss particles on the wall depend on the pitch angle of the tracing particle. To understand the trapped particle effects, more detailed experiments will be necessary with probe sets covering wider divertor footprint region.

In addition to these discussions based only on $\boldsymbol{B} \times \nabla B$ drift, we should pay attention to other possible drift (such as $\boldsymbol{E} \times \boldsymbol{B}$, $\boldsymbol{B} \times \nabla P$, $\boldsymbol{B} \times \nabla T$ drifts) effects taking into account the SOL plasma parameters. In order to investigate such effects and to understand the overall feature of the diverter plasma distribution, more detailed experimental data for the SOL and divertor plasmas are necessary.

Acknowledgements

The Heliotron J technical team is gratefully acknowledged for their excellent support to the experiments. This study is partly supported by the Collaboration Program of the Laboratory for Complex Energy Process, IAE, Kyoto University.

References

[1] X. Bonnin, W.L. Rowan, Nucl. Fusion 39 (1999) 1009.
[2] T. Mizuuchi et al., J. Nucl. Mater. 162–164 (1989) 105.
[3] T. Mizuuchi et al., J. Nucl. Mater. 266–269 (1999) 1139;
V.V. Chechkin et al., J. Plasma Fusion Res. Ser. 3 (2000) 197;
V.S. Voitsenya et al., these Proceedings (O-24).
[4] V.V. Chechkin et al., Nucl. Fusion 42 (2002) 192.
[5] M.S. Smirnova, Phys. Plasma 6 (1999) 897.
[6] V.V. Chechkin et al., IAEA TCM on Divertor Concept (Aix-an-Provence, France, September 2001), Nucl. Fusion, in preparation.
[7] T. Mizuuchi et al., J. Plasma Fusion Res. Ser. 3 (2000) 192.
[8] T. Mizuuchi et al., J. Nucl. Mater. 121 (1984) 3.
[9] N. Ohyabu et al., in: Plasma Physics and Controlled Nuclear Fusion Research, vol. 2, IAEA, Vienna, 1993, p. 605.
[10] T. Obiki et al., Nucl. Fusion 41 (2001) 833.
[11] F. Sano, T. Obiki, et al., J. Plasma Fusion Res. Ser. 3 (2000) 26.
[12] T. Obiki et al., 13th International Stellarator Conference, Canberra, 2002.
[13] W.L. Ang et al., Joint Conference of 12th International Toki Conference on Plasma Physics and Controlled Nuclear Fusion and Third General Scientific Assembly of Asia Plasma Fusion Association, Toki, 2001, Journal of Plasma Fusion Research Series, in press.
[14] T. Mizuuchi et al., J. Plasma Fusion Res. 77 (2001) 484 (in Japanese).
[15] T. Hirose, Master thesis, Graduate School of Energy Science, Kyoto University, 2002 (in Japanese).